J|A|C|S
ARTICLES

Published on Web 04/03/2008

Characterization of Alzheimer's-like Paired Helical Filaments from the Core Domain of Tau Protein Using Solid-State NMR Spectroscopy

Ovidiu C. Andronesi,[†,§] Martin von Bergen,[‡,#] Jacek Biernat,[‡] Karsten Seidel,[†] Christian Griesinger,[†] Eckhard Mandelkow,[‡] and Marc Baldus*[,†]

Department for NMR-based Structural Biology, Max Planck Institute for Biophysical Chemistry, 37077 Göttingen, Germany, and Max Planck Unit for Structural Molecular Biology at DESY, 22607 Hamburg, Germany

Received November 6, 2007; E-mail: maba@mpibpc.mpg.de

Abstract: The polymerization of the microtubule-associated protein tau into paired helical filaments (PHFs) represents one of the hallmarks of Alzheimer's disease. We employed solid-state nuclear magnetic resonance (NMR) to investigate the structure and dynamics of PHFs formed in vitro by the three-repeat-domain (K19) of protein tau, representing the core of Alzheimer PHFs. While N and C termini of tau monomers in PHFs are highly dynamic and solvent-exposed, the rigid segment consists of three major β-strands. Combination of through-bond and through-space ssNMR transfer methods with water-edited (^{15}N,^{13}C) and (^{13}C,^{13}C) correlation experiments suggests the existence of a fibril core that is largely built by repeat unit R3, flanked by surface-exposed units R1 and R4. Solid-state NMR, circular dichroism, and the fibrillization behavior of a K19 mutant furthermore indicate that electrostatic interactions play a central role in stabilizing the K19 PHFs.

Introduction

Tau protein is one of the key microtubule-associated proteins in neurons. Apart from its physiological function, the binding to and stabilization of microtubules, tau is found in pathologically aggregated forms in many "tauopathies", such as neurofibrillary tangles (NFTs) or neuropil threads (NPTs). In the case of Alzheimer's disease (AD), one observes two main types of aggregates, the intraneuronal NFTs containing "paired helical filaments" (PHFs) or "straight filaments" (SFs) assembled from hyperphosphorylated tau protein[1,2] and extracellular amyloid plaques consisting of filaments of the Aβ-peptide.[3] The progression and diagnosis of AD is highly correlated with the brain distribution of the intra-neuronal PHFs.[4] Investigating the fundamentals of tau polymerization is hence indispensable for identifying inhibitory conditions or compounds preventing formation of PHFs or oligomers, which may slow down or even reverse the degeneration of neurons in Alzheimer's disease.

While significant progress has been achieved in using magic-angle-spinning (MAS) solid-state NMR[5–16] and X-ray diffraction (XRD)[17,18] to characterize peptide and protein fibrils, little is known about the molecular details of tau PHFs. There are six main tau isoforms in the human brain that are developmentally regulated. The longest isoform (hTau40) consists of 441 residues and contains several important domains, such as the four pseudo-repeats R1−R4 (each ~31 amino acids; the second repeat R2 may be absent due to alternative splicing), which together with their proline-rich flanking regions (P1, P2) constitute the

[†] Max Planck Institute for Biophysical Chemistry.
[‡] Max Planck Unit for Structural Molecular Biology at DESY.
[§] Current address: Athinoula A. Martinos Center for Biomedical Imaging, Radiology Department, Massachusetts General Hospital, Harvard Medical School, 149 Thirteenth St., Boston, MA 02129.
[#] Current address: Helmholtz-Zentrum für Umweltforschung, Permoserstr. 15, D-04318 Leipzig, Germany.

(1) Trojanowski, J. Q.; Lee, V. M. *Nat. Neurosci.* **2005**, *8*, 1136–1137.
(2) Iqbal, K.; Alonso Adel, C.; El-Akkad, E.; Gong, C. X.; Haque, N.; Khatoon, S.; Pei, J. J.; Tanimukai, H.; Tsujio, I.; Wang, J. Z.; Grundke-Iqba, I. *J. Mol. Neurosci.* **2003**, *20*, 425–429.
(3) Selkoe, D. J. *Science* **2002**, *298*, 789–791.
(4) Braak, H.; Braak, E. *Acta Neuropathol. (Berlin)* **1991**, *82*, 239–259.
(5) Lansbury, P. T.; Costa, P. R.; Griffiths, J. M.; Simon, E. J.; Auger, M.; Halverson, K. J.; Kocisko, D. A.; Hendsch, Z. S.; Ashburn, T. T.; Spencer, R. G. S.; Tidor, B.; Griffin, R. G. *Nat. Struct. Biol.* **1995**, *2*, 990–998.
(6) Benzinger, T. L. S.; Gregory, D. M.; Burkoth, T. S.; Miller-Auer, H.; Lynn, D. G.; Botto, R. E.; Meredith, S. C. *Proc. Natl. Acad. Sci. U.S.A.* **1998**, *95*, 13407–13412.
(7) Laws, D. D.; Bitter, H. M. L.; Liu, K.; Ball, H. L.; Kaneko, K.; Wille, H.; Cohen, F. E.; Prusiner, S. B.; Pines, A.; Wemmer, D. E. *Proc. Natl. Acad. Sci. U.S.A.* **2001**, *98*, 11686–11690.
(8) Petkova, A. T.; Ishii, Y.; Balbach, J. J.; Antzutkin, O. N.; Leapman, R. D.; Delaglio, F.; Tycko, R. *Proc. Natl. Acad. Sci. U.S.A.* **2002**, *99*, 16742–16747.
(9) Jaroniec, C. P.; MacPhee, C. E.; Bajaj, V. S.; McMahon, M. T.; Dobson, C. M.; Griffin, R. G. *Proc. Natl. Acad. Sci. U. S. A.* **2004**, *101*, 711–716.
(10) Siemer, A. B.; Ritter, C.; Ernst, M.; Riek, R.; Meier, B. H. *Angew. Chem., Int. Ed.* **2005**, *44*, 2441–2444.
(11) Heise, H.; Hoyer, W.; Becker, S.; Andronesi, O. C.; Riedel, D.; Baldus, M. *Proc. Natl. Acad. Sci. U.S.A.* **2005**, *102*, 15871–15876.
(12) Ritter, C.; Maddelein, M.-L.; Siemer, A. B.; Luhrs, T.; Ernst, M.; Meier, B. H.; Saupe, S. J.; Riek, R. *Nature* **2005**, *435*, 844–848.
(13) Iwata, K.; Fujiwara, T.; Matsuki, Y.; Akutsu, H.; Takahashi, S.; Naiki, H.; Goto, Y. *Proc. Natl. Acad. Sci. U.S.A.* **2006**, *103*, 18119–18124.
(14) Ferguson, N.; Becker, J.; Tidow, H.; Tremmel, S.; Sharpe, T. D.; Krause, G.; Flinders, J.; Petrovich, M.; Berriman, J.; Oschkinat, H.; Fersht, A. R. *Proc. Natl. Acad. Sci. U.S.A.* **2006**, *103*, 16248–16253.
(15) van der Wel, P. C. A.; Lewandowski, J. R.; Griffin, R. G *J. Am. Chem. Soc.* **2007**, *129*, 5117–5130.
(16) Chimon, S.; Shaibat, M. A.; Jones, C. R.; Calero, D. C.; Aizezi, B.; Ishii, Y. *Nat. Struct. Mol. Biol.* **2007**, *14*, 1157–1164.

10.1021/ja7100517 CCC: $40.75

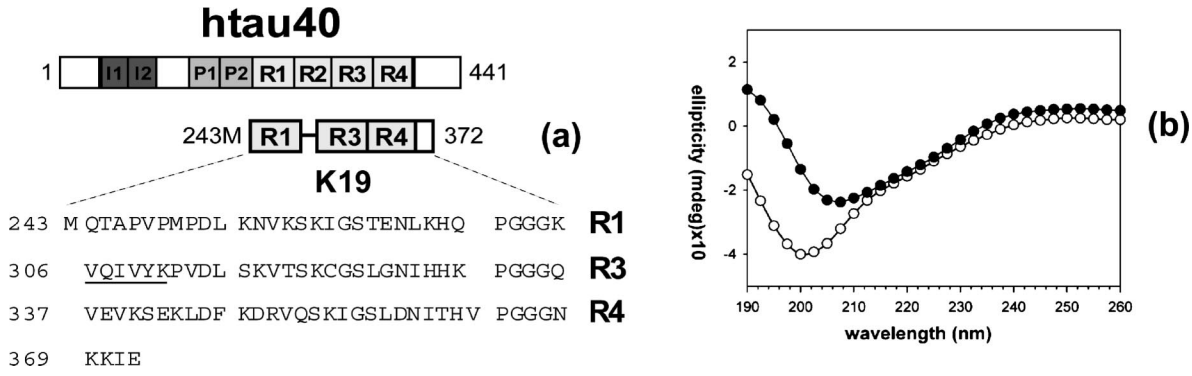

Figure 1. (a) The longest tau isoform htau40, highlighting the repeat domains and the K19 sequence. (b) CD spectra obtained on K19 PHFs at pH 7 (●) and at pH 2 (○). The hexapeptide motif is underlined.

microtubule-binding domain. In contrast to the Aβ peptide, microtubule-associated protein tau is a highly soluble protein largely devoid of hydrophobic amino acids. In addition, the microtubule-binding domain of tau contains an excess of positively charged amino acids. These properties explain the "natively unfolded" character of soluble tau protein.[19,20] Electron microscopy (EM) micrographs on full-length tau filaments purified from AD brains or assembled in vitro show a "core" region and a "fuzzy coat".[21] The aggregation of tau is highly accelerated by the addition of polyanions that contain an extended negative charge[22] and leads to a conformational switch from a mostly random coil to a β sheet structure in a limited region of the repeat domain surrounding the "hexapeptide motifs".[23,24] The latter conclusion is consistent with circular dichroism (CD), Fourier-transform infrared (FTIR), XRD, and solution NMR studies.[25–29] X-ray powder diffraction reveals a *cross-*β structure[23,30] homologous to other amyloidogenic peptides and proteins.[31] Protease digestion and solvent accessibility studies further determined that the core of PHF is mainly built from the microtubule-binding domains, such that R2 and R3 are most deeply buried within the PHF structure.[32,33] While structural information on the PHF fibril core was obtained by different techniques, such as X-ray fiber diffraction,[33,34] electron paramagnetic resonance (EPR),[35,36] fluorescence, CD, and FTIR spectroscopy,[22,37] insight into the structural arrangement of tau PHFs on the residue-specific level is still scarce.

We utilized solid-state NMR to study the fibril structure of PHFs reassembled in vitro from the repeat domain construct K19 (99 residues), of tau which comprises three repeats of 31 residues[38] (corresponding to the juvenile form of tau, Figure 1). To examine the structural arrangement of PHFs grown from uniformly (^{13}C,^{15}N)-labeled protein, we combined solid-state NMR methods that permit the structural analysis of uniformly labeled proteins under MAS conditions[39] with techniques that probe different degrees of molecular mobility.[40] In addition, we monitored the molecular topology in protein fibrils relative to a mobile aqueous environment. Our study identifies dynamic and rigid segments of the fibril, leads to the identification of three major β-strand segments in repeat unit R1, R3, and R4, and suggests possible molecular arrangements that are compatible with EM and EPR data. In accordance with the spectroscopic data, CD experiments and studies of a K19 mutant speak in favor of a dominant influence of electrostatic interactions. This observation may provide novel insight into the generic principles of protein aggregation and may lead to novel approaches for identifying inhibitory conditions or compounds preventing tau PHF or oligomer formation.

Materials and Methods

Expression and Purification of (^{13}C,^{15}N)-Labeled K19 Tau Construct. Uniformly (^{13}C,^{15}N)-labeled K19 protein was produced by growing BL21(DE3) bacteria in rich growth medium derived from chemolithoautotrophic bacteria labeled with ^{13}C and ^{15}N

(17) Nelson, R.; Sawaya, M. R.; Balbirnie, M.; Madsen, A. O.; Riekel, C.; Grothe, R.; Eisenberg, D. *Nature* **2005**, *435*, 773–778.
(18) Eisenberg, D.; Nelson, R.; Sawaya, M. R.; Balbirnie, M.; Sambashivan, S.; Ivanova, M. I.; Madsen, A. O.; Riekel, C. *Acc. Chem. Res.* **2006**, *39*, 568–575.
(19) Lee, G.; Cowan, N.; Kirschner, M. *Science* **1988**, *239*, 285–288.
(20) Schweers, O.; Schonbrunn-Hanebeck, E.; Marx, A.; Mandelkow, E. *J. Biol. Chem.* **1994**, *269*, 24290–24297.
(21) Crowther, T.; Goedert, M.; Wischik, C. M. *Ann. Med.* **1989**, *21*, 127–132.
(22) von Bergen, M.; Barghorn, S.; Biernat, J.; Mandelkow, E.-M.; Mandelkow, E. *Biochim. Biophys. Acta* **2005**, *1739*, 158–166.
(23) von Bergen, M.; Friedhoff, P.; Biernat, J.; Heberle, J.; Mandelkow, E. M.; Mandelkow, E. *Proc. Natl. Acad. Sci. U.S.A.* **2000**, *97*, 5129–5134.
(24) von Bergen, M.; Barghorn, S.; Li, L.; Marx, A.; Biernat, J.; Mandelkow, E. M.; Mandelkow, E. *J. Biol. Chem.* **2001**, *276*, 48165–48174.
(25) Goux, W. J.; Kopplin, L.; Nguyen, A. D.; Leak, K.; Rutkofsky, M.; Shanmuganandam, V. D.; Sharma, D.; Inouye, H.; Kirschner, D. A. *J. Biol. Chem.* **2004**, *279*, 26868–26875.
(26) Barghorn, S.; Davies, P.; Mandelkow, E. *Biochemistry* **2004**, *43*, 1694–1703.
(27) Mukrasch, M. D.; Biernat, J.; von Bergen, M.; Griesinger, C.; Mandelkow, E.; Zweckstetter, M. *J. Biol. Chem.* **2005**, *280*, 24978–24986.
(28) Sillen, A.; Wieruszeski, J. M.; Leroy, A.; Younes, A. B.; Landrieu, I.; Lippens, G. *J. Am. Chem. Soc.* **2005**, *127*, 10138–10139.
(29) Eliezer, D.; Barre, P.; Kobaslija, M.; Chan, D.; Li, X.; Heend, L. *Biochemistry* **2005**, *44*, 1026–1036.
(30) Berriman, J.; Serpell, L. C.; Oberg, K. A.; Fink, A. L.; Goedert, M.; Crowther, R. A. *Proc. Natl. Acad. Sci. U.S.A.* **2003**, *100*, 9034–9038.
(31) Sunde, M.; Serpell, L. C.; Bartlam, M.; Fraser, P. E.; Pepys, M. B.; Blake, C. C. *J. Mol. Biol.* **1997**, *273*, 729–739.
(32) Li, H.; von Bergen, M.; Mandelkow, E.-M.; Mandelkow, E. *J. Biol. Chem.* **2002**, *277*, 41390–41400.
(33) vonBergen, M.; Barghorn, S.; Muller, S. A.; Pickhardt, M.; Biernat, J.; Mandelkow, E. M.; Davies, P.; Aebi, U.; Mandelkow, E. *Biochemistry* **2006**, *45*, 6446–6457.
(34) Goux, W. J. *Biochemistry* **2002**, *41*, 13798–13806.
(35) Margittai, M.; Langen, R. *Proc. Natl. Acad. Sci. U. S. A.* **2004**, *101*, 10278–10283.
(36) Margittai, M.; Langen, R. *J. Biol. Chem.* **2006**, *281*, 37820–37827.
(37) Barghorn, S.; Zheng-Fischhofer, Q.; Ackmann, M.; Biernat, J.; von Bergen, M.; Mandelkow, E. M.; Mandelkow, E. *Biochemistry* **2000**, *39*, 11714–11721.
(38) Wille, H.; Drewes, G.; Biernat, J.; Mandelkow, E. M.; Mandelkow, E. *J. Cell Biol.* **1992**, *118*, 573–584.
(39) Baldus, M. *Prog. Nucl. Magn. Reson. Spectrosc.* **2002**, *41*, 1–47.
(40) Andronesi, O. C.; Becker, S.; Seidel, K.; Heise, H.; Young, H. S.; Baldus, M. *J. Am. Chem. Soc.* **2005**, *127*, 12965–12974.

isotopes (Silantes, Munich, Germany). Protein was purified as described,[41] dialyzed against 50 mM ammonium acetate (NH_4Ac), pH 7.0, and concentrated to 1–1.5 mM.

PHF Assembly in Vitro. PHFs were assembled from K19 tau protein as described.[23,42] For the purpose of our experiments, samples were prepared in which isotope-labeled monomers were diluted with unlabeled monomers in a ratio of 1:10 in order to probe the 3D fold of monomers inside the fibers. Assembly was performed in 50 mM NH_4Ac, pH 7.0, at various concentrations (ranging from 100 to 500 mM) with a ratio of protein:heparin (MW 6000 Da) of 4:1 for at least 3 days at 37 °C. The polymerization reaction mixture was centrifuged at 40000*g*, and the pellet was washed twice with polymerization buffer. The suspension was pelleted again before it was suspended in a small volume of 50 mM NH_4Ac, pH 7.0. Polymerization products were checked by negative stain EM.

Circular Dichroism Spectroscopy. The content of secondary structure was analyzed by CD spectroscopy with a Jasco model 810 spectrometer (Gross-Umstadt, Germany). Measurements were performed at protein concentrations of 0.05 mg/mL. As a standard condition, the protein was dialyzed against 20 mM sodium phosphate buffer, pH 7. For studies of PHF stability, the concentrations of GdHCl were varied, different pH values were obtained by using different buffers, or other reagents like glycerol or propanol were added. Spectra were taken in the range of 185–260 nm, with a scanning speed of 50 nm/min, a response time of 2 s, and a slit width of 1 nm. For each output curve, three spectra were accumulated. The spectra were smoothed by the Savitzky−Golay algorithm with a convolution width of 17 using "spectra analysis" software from Jasco.

Solid-State NMR Experiments and Analysis. All NMR experiments were conducted using 4 mm triple-resonance (^1H,^{13}C,^{15}N) probeheads at static magnetic fields of 9.4, 14.1, and 18.8 T, corresponding to 400, 600, and 800 MHz proton resonance frequencies (Bruker Biospin, Karlsruhe, Germany). Through-space transfer experiments involved broadband (^1H,^{13}C) and chemical-shift selective[43] (^{15}N,^{13}C) Hartmann–Hahn cross-polarization (SPECIFIC-CP) schemes. SPINAL64[44] proton decoupling was applied during through-space correlation experiments using radio frequency fields of 60–70 kHz. Sequential (^{15}N,^{13}C) resonance assignments of the rigid core were obtained by combining 2D NCACX/NCOCX data with results of (^{13}C,^{13}C) correlation experiments performed under weak coupling conditions, where sequential polarization transfer among carbon spins is facilitated.[45] MAS rates between 8 and 15 kHz were employed, and the sample temperature (5 °C, calibrated using reference compounds under comparable experimental conditions) was controlled using an external heater. We expect an error in sample temperature of ±3 °C. Selection and assignment of regions with high mobility was achieved using pulse schemes described previously.[40] During through-bond experiments, 10 kHz proton decoupling was realized employing the GARP[46] scheme. To study the fibril−water interface, NMR signals of mobile protons were selected using a relaxation filter.[47] During a subsequent spin diffusion time, polarization transfer to the immobilized biomolecule was established. In the initial rate regime,[48] the resulting polarization transfer characteristics are sensitive to the distance between a given protein spin in the interior of the molecular complex and the surrounding H_2O environment. For the purpose of our studies, we extended existing pulse schemes by an additional (C,C) spin-diffusion or (N,C) SPECIFIC-CP mixing unit, which permits recording a two-dimensional (2D) correlation map of all protein resonances detectable for a given diffusion time (see Supporting Information). As described earlier,[48] proton exchange and NOE cross relaxation represent two alternative mechanisms for polarization transfer between water and solid surfaces. While such effects have been observed in microcrystalline proteins,[49,50] the experimental details (sample conditions, pulse schemes, and CP contact times) differ substantially from our experiments. In addition, these mechanisms can be distinguished by their dependence on temperature which, since transfer rates decrease at higher temperatures, favors dipolar transfer in our case (data not shown), and the diffusion constants obtained here compare favorably to values reported in the literature (vide infra).

Secondary chemical shifts were used to identify β-strand regions of K19 fibrils. As a complementary method, backbone proton–proton distances were probed indirectly using an NHHC[51] scheme. Experimentally, a (^1H,^1H) mixing time of 80 μs, bracketed by short (^1H,X) CP transfers for contact times of 50 μs (X = ^{13}C) and 60 μs (X = ^{15}N), was used. Cross peaks for this mixing time are dominated by $N^{i+1}H-HC\alpha^i$ contacts resulting from neighboring amino acids located in β-strands (with glycine Cα atoms being an exception).

Results and Discussion

Secondary Structure and Dynamics of K19 Fibrils. In addition to full-length tau (Figure 1a), PHFs can be prepared from tau domains containing three or four repeats that display the major features of PHFs purified from AD brains. In particular, the three-repeat-domain construct K19 (99 residues, Figure 1a) gives rise to twisted filaments in electron micrographs similar to full-length tau[33] and is characterized by a broad minimum at 205 nm in the CD spectrum. These data indicate a mixture of random coil and β-structure at pH 7, which arises from the partial conversion of random coil to β-structure during PHF assembly[23] (Figure 1b).

To obtain de novo sequential ssNMR resonance assignments of uniformly isotope-labeled (in the following abbreviated by U-[^{13}C,^{15}N]) K19 PHFs, we used a set of 2D correlation experiments that establish polarization transfer using through-bond or through-space interactions for mobile and rigid protein segments, respectively.[40] As an example, Figure 2 shows results of a 2D through-bond (^1H,^{13}C) (Figure 2a) and a (^{13}C,^{13}C) dipolar spin diffusion experiment (conducted under weak coupling conditions,[45] Figure 2b) on U-[^{13}C,^{15}N] K19 PHFs. Dipolar-based correlation spectra exhibit ^{13}C and ^{15}N line widths ranging from 1 to 2 ppm that are larger than those seen in the through-bond experiments.

A subsequent analysis of a series of CC and NC 2D spectra, such as the NCA-type experiments[39,40] shown in Figure 2c,d and the NCOCA-type spectra shown in Figure 3, led to de novo assignments of 20 residues in the mobile N and C termini of K19 PHFs and 43 amino acids in the rigid segments (see Table 1, Supporting Information). For mobile K19 fibril segments (Figure 2a), cross peaks resulting from (^{13}C,^{13}C) through-bond

(41) Barghorn, S.; Biernat, J.; Mandelkow, E. *Methods Mol. Biol.* **2005**, *299*, 35–51.
(42) Friedhoff, P.; Schneider, A.; Mandelkow, E. M.; Mandelkow, E. *Biochemistry* **1998**, *37*, 10223–10230.
(43) Baldus, M.; Petkova, A. T.; Herzfeld, J.; Griffin, R. G. *Mol. Phys.* **1998**, *95*, 1197–1207.
(44) Fung, B. M.; Khitrin, A. K.; Ermolaev, K. *J. Magn. Reson.* **2000**, *142*, 97–101.
(45) Seidel, K.; Lange, A.; Becker, S.; Hughes, C. E.; Heise, H.; Baldus, M. *Phys. Chem. Chem. Phys.* **2004**, *6*, 5090–5093.
(46) Shaka, A. J.; Barker, P. B.; Freeman, R. *J. Magn. Reson.* **1985**, *64*, 547–552.
(47) Edzes, H. T.; Samulski, E. T. *Nature* **1977**, *265*, 521–523.
(48) Kumashiro, K. K.; Schmidt-Rohr, K.; Murphy, O. J.; Ouellette, K. L.; Cramer, W. A.; Thompson, L. K. *J. Am. Chem. Soc.* **1998**, *120*, 5043–5051.
(49) Lesage, A.; Böckmann, A. *J. Am. Chem. Soc.* **2003**, *125*, 13336–13337.
(50) Lesage, A.; Emsley, L.; Penin, F.; Bockmann, A. *J. Am. Chem. Soc.* **2006**, *128*, 8246–8255.
(51) Lange, A.; Seidel, K.; Verdier, L.; Luca, S.; Baldus, M. *J. Am. Chem. Soc.* **2003**, *125*, 12640–12648.
(52) Luca, S.; Filippov, D. V.; van Boom, J. H.; Oschkinat, H.; de Groot, H. J. M.; Baldus, M. *J. Biomol. NMR* **2001**, *20*, 325–331.

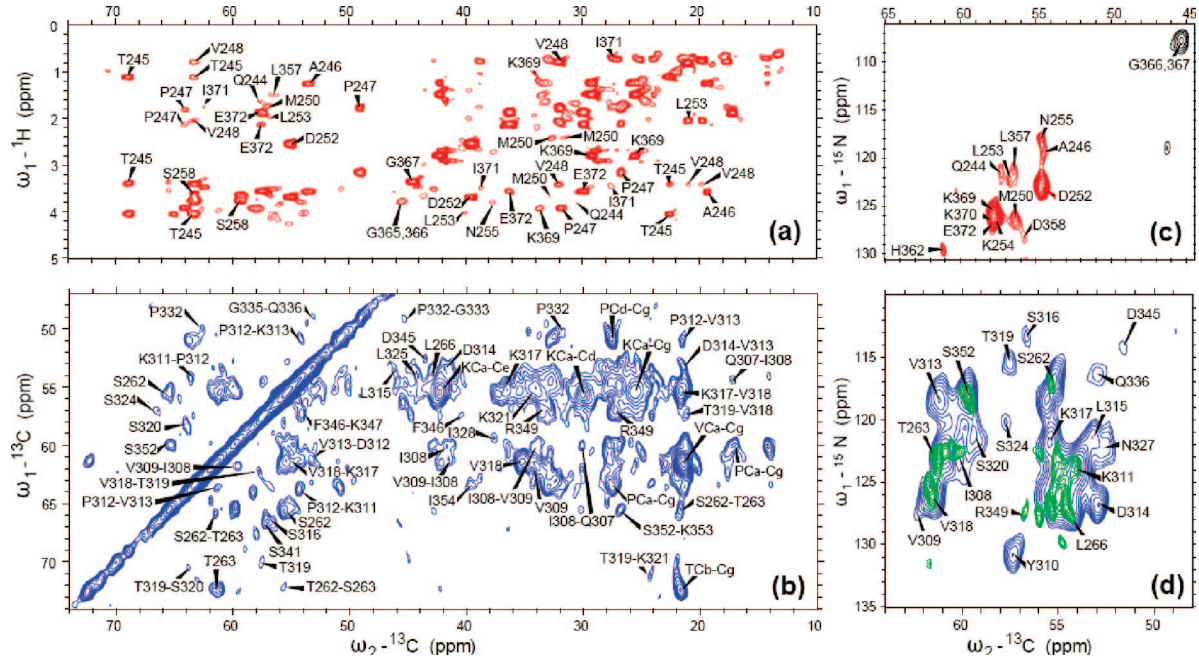

Figure 2. Through-bond (a,c, red) and through-space (b,d, blue) 2D ssNMR correlation spectra on U-[^{13}C,^{15}N] K19, probing mobile and rigid filament segments, respectively. Spectra shown relate to (a) HCC INEPT-TOBSY,[40] (b) CC spin-diffusion spectrum under weak couplings conditions,[45] and NCA[40] (c,d) experiments. In (d), an H_2O-edited NCA experiment (green) using a proton–proton mixing time of 6 ms is included for comparison. Selected intra- and inter-residue correlations are highlighted. Further experimental conditions are given in Table 2 (Supporting Information).

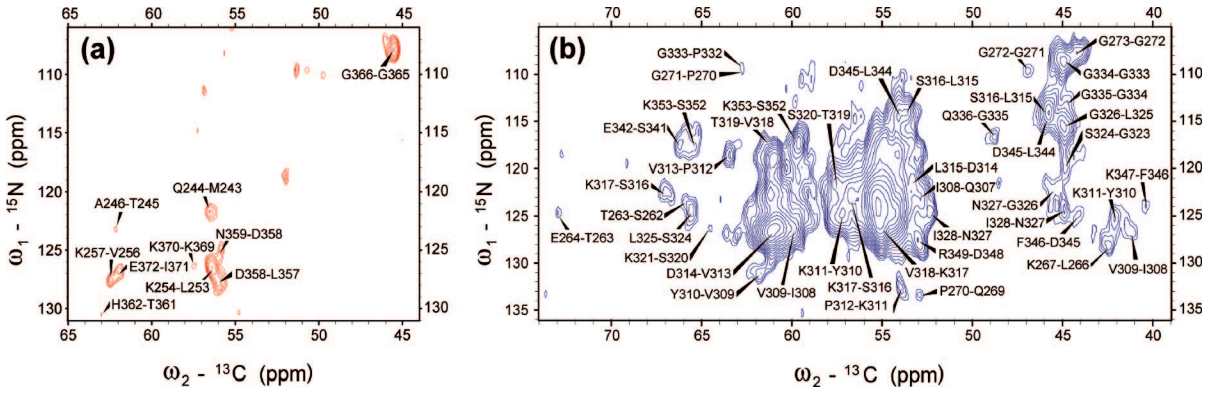

Figure 3. 2D NCOCA spectra: (a) INEPT-TOBSY experiment for mobile termini and (b) CP-SD experiment for rigid core.

transfer allowed for direct assignment for Ala246 due to its unique presence in the K19 amino acid sequence.

In Figure 4b, these resonance assignments were used to compute secondary chemical shifts (as defined in ref 52) that are sensitive to protein backbone structure[53] along the K19 amino acid sequence (Figure 4a). Accordingly, α-helical and β-strand protein segments are characterized by positive and negative values of $\Delta\delta$, respectively, that exceed the natural line width (i.e, $|\Delta\delta| > 1$ ppm). For residues with incomplete Cα or Cβ resonance assignments, $\Delta\delta$ was set to zero. Remarkably, $\Delta\delta$ parameters seen for mobile residues (indicated in red) are largely positive for the N terminus (252–258) and for the segment 358–363 of R4. In contrast to the terminal segments of K19, secondary chemical shifts seen for several residues in R1 (above G260), the entire R3 repeat except for four residues, and eight residues of R4 (below V350) exhibit $\Delta\delta$ values < -1 ppm, consistent with a strong β-strand character. Secondary chemical shift data obtained for the PGGG motifs in R1 and R3 suggest that these segments are not part of extended segments of the K19 fibrils.

To look at an independent parameter that is sensitive to protein secondary structure, we performed an NHHC experiment under conditions where β-strand regions should dominate the spectrum (see, e.g., refs 51, 54). Although an identification of individual correlations is hampered by spectral resolution (see Supporting Information), the data are most compatible with β-strand regions indicated in Figure 4c. β-Strands deduced from conformation-dependent chemical shifts (Figure 4b) or proton–proton distances (Figure 4c) are summarized in Figure 4c, suggesting that the rigid part of K19 monomers contains three major β-strands: (i) a short (262–267) stretch at the end of the first repeat (which we will abbreviate in the following as βR1), (ii) residues 307–328 (except for Pro312) in the third repeat (βR3′,βR3), and (iii) amino acids 336–354 in the fourth repeat (βR4′,βR4). Since proline is know to act as a local β-strand

(53) Wishart, D. S.; Sykes, B. D. *Nucl. Magn. Reson. C* **1994**, *239*, 363–392.
(54) Seidel, K.; Etzkorn, M.; Heise, H.; Becker, S.; Baldus, M. *Chembiochem* **2005**, *6*, 1638–1647.

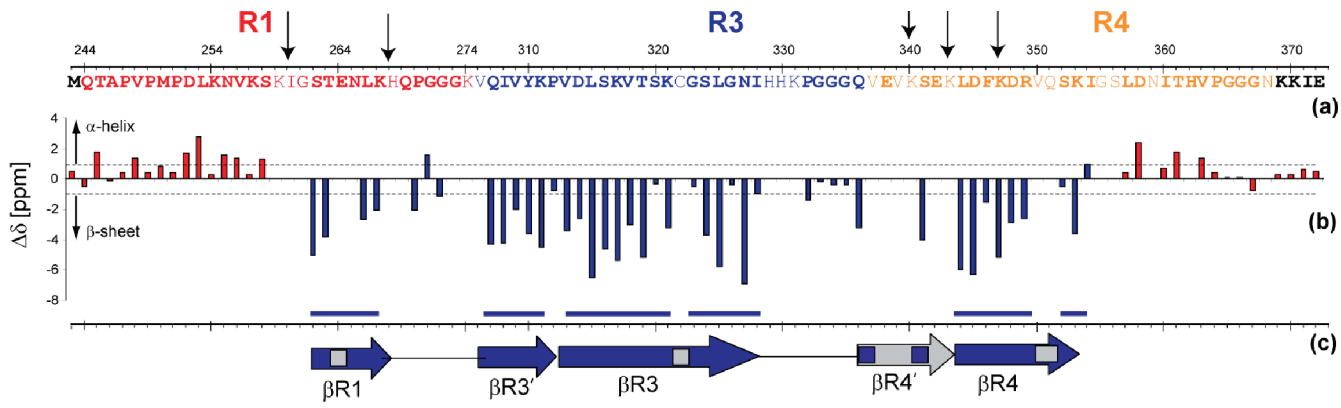

Figure 4. (a) Sequence of tau construct K19 comprising repeats R1, R3, and R4 (given in different colors), corresponding to the fetal form of protein tau. ssNMR assignments were obtained for residues indicated in bold (see also Supporting Information). Arrows point to trypsin-sensitive sites in tau PHFs.[33] (b) Secondary chemical shifts of rigid (blue) and mobile (red) residues. (c) β-Sheet regions confirmed by NHHC data (see Supporting Information). β-Strands compatible with the chemical shift analysis or the NHHC data are indicated. Gray regions are not fully assigned.

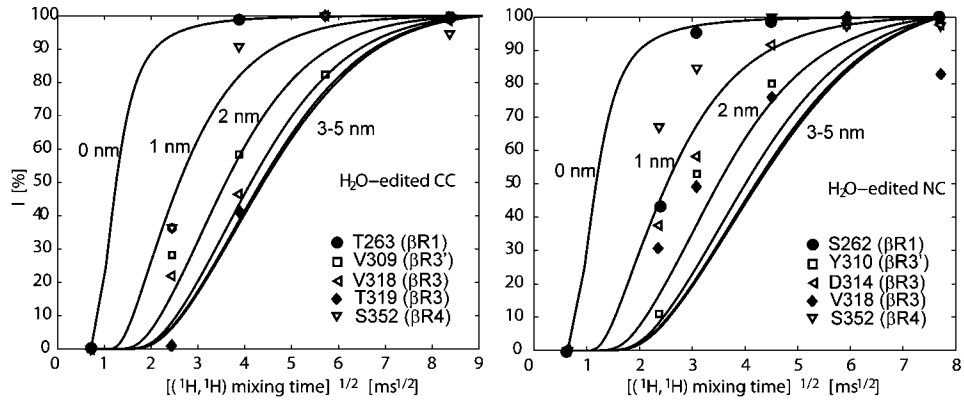

Figure 5. Experimental results of H_2O-edited (^{13}C,^{13}C) (left) and (^{15}N,^{13}C) (right) correlation experiments on U-[^{13}C,^{15}N] K19 PHFs. Data were recorded at 600 (C,C) and 400 (N,C) MHz, using mixing times of 3, 10, 25, and 70 ms (C,C) and 3, 6, 15, 28, and 50 ms (N,C), respectively. In both cases, a T_2 filter time of 2.5 ms (δ = 1.25 ms; see Supporting Information) was used. Theoretical buildups are computed for each nanometer penetration depth toward the fibril interior.

breaker,[12,55] the rather small secondary chemical shift for Pro 312 may reflect interruption of βR3 as indicated in Figure 4. In the latter segment (βR4′), an unequivocal assignment of all residues was complicated by spectral overlap. However, the observed cross peak patterns for all Val residues exhibit β-strand character which suggests, together with the assignments for Q336, S342, and E343, formation of an additional β-strand (βR4′). (βR3′,βR3) contains one of the assembly-promoting hexapeptide motifs identified previously on biochemical grounds,[23] and (βR4′,βR4) encloses residues 337–342 located equivalently in R4. These strands also contain residues V306-L315 and Q336-D345 that exhibited nascent β-structure in soluble K19 monomers.[27] On the other hand, a similar correlation of β-structure between K19 monomers and PHFs is not obtained for R1 and is not seen for the remaining segments of R3 and R4. Furthermore, the connecting segments βR1−βR3 and βR3−βR4 consist of PGGG motifs that exhibit ssNMR data typically found for protein loops or turns. Note that the trypsin-sensitive sites in K19 PHFs[33] (indicated by arrows in Figure 3) are found in close proximity of the mobile−rigid PHF interface, as diagnosed by ssNMR.

Supramolecular Arrangement of K19 PHFs. To further characterize the fibril structure, we implemented (N,C) and (C,C) 2D ssNMR correlation experiments that probe rigid fibril regions in the vicinity of an aqueous environment (see also Materials and Methods). Here, magnetization transfer occurs first from mobile water protons to the fibril surface and subsequently via proton-mediated spin diffusion. As an example, an H_2O-edited NCA experiment (green) is compared to the standard NCA[39] data (blue) in Figure 2d and reveals significant differences between the two spectra. We recorded a series of such 2D correlation experiments and monitored the signal intensity as a function of the proton–proton mixing time. These data are compared for a selected set of residues to theoretical spin diffusion buildup curves in Figure 5. In the theoretical calculations, diffusion constants of D = 0.04 nm^2/ms (water–protein interface) and D = 1.2 nm^2/ms (interior of fibril) were assumed, which are in good agreement with values previously seen in organic solids.[48] In the initial rate regime, significant differences are observed between residues located in strands (βR4′,βR4), βR1, and (βR3′,βR3), respectively.

Comparison of this result to trypsin-sensitive sites in tau PHFs previously identified[33] (Figure 4) strongly suggests that strands βR1 and (βR4′,βR4) are more solvent-exposed than the (βR3′,βR3) segment. This conclusion is also in agreement with results of through-bond HHC correlation experiments,[40] revealing that the mobile termini are also in close contact with bulk water. These findings are summarized in Figure 6a, where

(55) Wood, S. J.; Wetzel, R.; Martin, J. D.; Hurle, M. R. *Biochemistry* **1995**, *34*, 724–730.

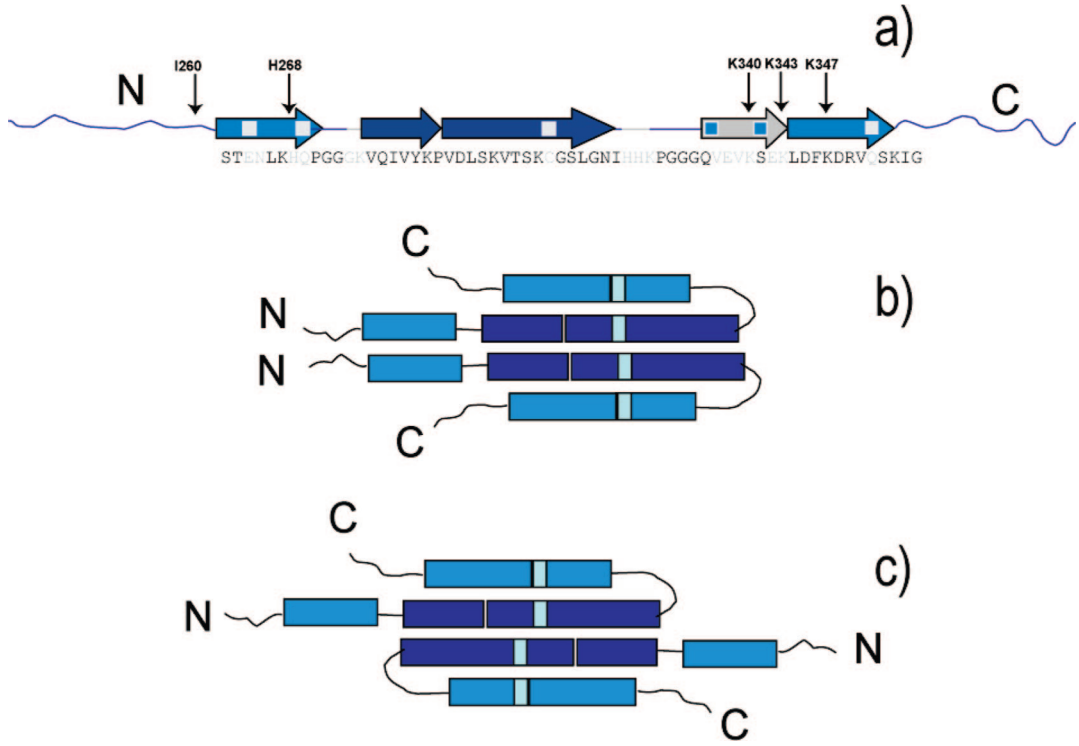

Figure 6. (a) Comparison of ssNMR analysis and previous studies based on limited digestion of PHFs by trypsin.[33] Tentative β-strand regions are given by arrows. Sequences lying at the surface or within the core of K19 PHFs are indicated by light and dark blue colors, respectively. Gray regions are not completely assigned. Note that trypsin-sensitive sites (arrows) occur only in surface regions. (b,c) Structural models of a K19 PHF dimer that leads to complete protection of the R3 β-strand in a parallel or antiparallel manner. Charge-swapping mutation sites are given in light blue (K317E in R3, E342K in R4). Thin bars reflect possible β-strand interruption in R3 at P312.

shielded and interface regions of the core unit are given in dark and light blue, respectively.

In the absence of further long-range and intermolecular constraints, a high-resolution structural model cannot be obtained. However, the data obtained here can be used to speculate about possible molecular arrangements that are compatible with our spectroscopic analysis and previous findings. Considering the length of the β-strand segments found in R1, R3, and R4, it seems unlikely that protection of the R3 strand can be accomplished in a monomer arrangement. Possible dimer folds that would allow for such protection are given in Figure 6. All ssNMR spectra discussed here were obtained on diluted samples to reduce complication of the data analysis by intermolecular polarization transfer. For this reason, discrimination between a parallel (Figure 6b) or antiparallel (Figure 6c) arrangement of K19 dimers along the fibril axis is not possible.

Comparison to Other Results. First, the largely β-strand character of the K19 monomer unit is consistent with XRD studies that found a cross structure in PHFs where the β-beta strands run roughly perpendicularly to the fiber axis.[24,25,30] The strong equatorial reflection at about 1 nm indicates the existence of an intersheet stacking, requiring at least two β-sheets. According to previous STEM studies of PHFs from Alzheimer brain or tau constructs such as K19, the number of molecules per nanometer is approximately four.[33] This is consistent with the structural models of Figure 6, because the two molecules per cross-sectional layer would be separated from the next layer by $\sim$0.47 nm, giving roughly four molecules per nanometer in the axial direction.

Protease digestion and solvent-accessibility studies further determined that the core of PHF is mainly built from the microtubule-binding domains, such that R2 and R3 are most deeply buried within the PHF structure.[32,33] In particular, trypsin-sensitive exposed sites in K19 fibrils are found[33] near the end of R4 at residues K340, K343, and K347 (Figure 6a, arrows). The same argument holds for further trypsin-sensitive sites that lie at the lysines preceding I260 and H268 near the end of R1. In qualitative agreement with these results, Figures 6 reveals that these protein residues are all located on the exterior side of K19 PHFs and do not constitute the fibril core. The existence of a macromolecular organization in which K19 fibrils form water-filled nanotubes[56] would hence be incompatible with our data. Further support for the supramolecular organization of the tau fibril with the R3 repeat in its core comes from the high β-sheet propensity of the R3 repeat residues 305−315, which promote the formation of cross β-structure.[24]

On the level of individual residues, the structural models must be stabilized by side-chain/side-chain interactions, possibly including the formation of salt bridges. Notably, the existence of such salt bridges is consistent with two resolved ^{15}N ssNMR side-chain resonances for Lys that are known to vary upon changes in protonation[57] (data not shown). For amyloid fibrils such as Aβ that are stabilized by hydrophobic interactions, fibril formation is possible for a wide pH range.[58] On the other hand, if salt bridges are important for PHF stabilization, changes in pH should affect the filament strength. This conclusion is supported by CD experiments (Figure 1b) at variable pH. K19 PHFs assembled at pH 7 exhibited a broad minimum at 205

(56) Perutz, M. F.; Finch, J. T.; Berriman, J.; Lesk, A. *Proc. Natl. Acad. Sci. U.S.A.* **2002**, *99*, 5591–5595.
(57) Zhu, L. Y.; Kemple, M. D.; Yuan, P.; Prendergast, F. G. *Biochemistry* **1995**, *34*, 13196–13202.
(58) Petkova, A. T.; Yau, W. M.; Tycko, R. *Biochemistry* **2006**, *45*, 498–512.

nm, indicating a mixture of random coil and β-structure. At pH 2, PHFs do not assemble de novo, and preassembled PHFs become dissolved again, leading to a minimum at 200 nm in the CD spectrum typical of random coil conformation.[59] Such effects would be consistent with the protonation of Glu and Asp at pH 2 and the disappearance of the salt bridges between Asp/Glu and Lys.

As an independent measure of the potential influence of salt bridges, we investigated the fibril formation of a K19 double mutant, i.e., K317E-E342K, in which the electrostatic side-chain character is reversed. According to our model, the considered residues should be in relatively close spatial proximity (Figure 6). Indeed, this mutant protein displays similar fibril morphologies (data not shown). Although we cannot exclude that such electrostatic interactions are intermolecular, this result supports structural models in which the two mutated residues are in close spatial proximity either due to the monomer arrangement or within the supramolecular organization of the K19 PHFs. Such structures are fully compatible with a central R3 segment that is tightly packed and forms parallel in-register structure, as predicted by EPR of site-directed tau mutants carrying spin labels.[35,36] Correspondingly, a β-sandwich which has been deduced from NMR data obtained for Aβ(1–40),[60] Aβ(1–42),[61] a 22-residue peptide fragment of the β2-microglobulin (β2m),[13] and a WW domain of human CA150[14] would be possible (Figure 6b,c).

Finally, the other driving force of PHF formation is assumed to be hydrophobic interactions, because polymerization of tau is favored with increasing temperatures.[42] Additionally, mutants of tau occurring in frontotemporal dementias which are capable of increasing the amphipathic nature of sequences around the hexapeptide motifs show faster aggregation rates.[37] In qualitative agreement with this notion, the core unit of the K19 PHF contains a variety of hydrophobic residues that may contribute to PHF stability.

Conclusions

The polymerization of the microtubule-associated protein tau into paired helical filaments (PHFs) is one of the hallmarks of Alzheimer's disease. We employed solid-state NMR to investigate the structure and dynamics of PHFs formed in vitro by the three-repeat-domain (K19) of protein tau. Together with α-synuclein,[11] this 99-amino-acid construct represents the largest fibrillar proteins for which sequential ssNMR resonance assignments have been obtained to date. While N and C termini of K19 fibrils are highly dynamic and solvent-exposed, the rigid segment consists of three major β-strands (βR1, βR3′/βR3, and βR4′/βR4). Our study suggests that the minimal structural unit of K19 filaments comprises two molecules in which the central βR3 strand represents the PHF interior.

In the cases of Aβ,[8] PrP,[62] and α-synuclein,[11] hydrophobic protein sequences are considered to play the dominant role in protein aggregation. For example, the structured core of Aβ fibrils[8] consists of about 56% hydrophobic residues and contains only 10% charged amino acids. In contrast, our study on K19 PHFs suggests that the rigid core region of K19 PHFs contains about an equal fraction (30%) of charged and hydrophobic amino acids. Together with what is known for the aggregation of polyglutamine[63] and yeast prions,[64] where polar interactions are believed to drive protein misfolding and the recent model of a steric zipper,[17] our study suggests that accounting for protein sequence diversity is crucial for determining the mechanism of molecular aggregation and its pharmacological intervention on a structural level.

Acknowledgment. We thank Sabrina Hübschmann, Bianca Wichmann, and Brigitta Angerstein for excellent technical assistance. Discussions with Dr. H. Heise are acknowledged. This work was conducted within the scientific scope of the DFG Center for Molecular Physiology of the Brain (CMPB) and the Graduiertenkolleg GRK 782 in Göttingen.

Supporting Information Available: Sequential ssNMR resonance assignments of K19 PHFs, experimental conditions of ssNMR experiments, a 2D NHHC spectrum, the pulse scheme for H_2O-edited NCA correlation spectroscopy, and further information regarding the theoretical analysis of the H_2O-edited correlation spectra. This material is available free of charge via the Internet at http://pubs.acs.org.

JA7100517

(59) Fasman, G. D. *Trends Biochem. Sci.* **1989**, *14*, 295–299.
(60) Petkova, A. T.; Ishii, Y.; Balbach, J. J.; Antzutkin, O. N.; Leapman, R. D.; Delaglio, F.; Tycko, R. *Proc. Natl. Acad. Sci. U.S.A.* **2002**, *99*, 16742–16747.
(61) Luhrs, T.; Ritter, C.; Adrian, M.; Riek-Loher, D.; Bohrmann, B.; Dobeli, H.; Schubert, D.; Riek, R. *Proc. Natl. Acad. Sci. U.S.A.* **2005**, *102*, 17342–17347.
(62) Tagliavini, F.; Prelli, F.; Verga, L.; Giaccone, G.; Sarma, R.; Gorevic, P.; Ghetti, B.; Passerini, F.; Ghibaudi, E.; Forloni, G.; Salmona, M.; Bugiani, O.; Frangione, B. *Proc. Natl. Acad. Sci. U.S.A.* **1993**, *90*, 9678–9682.
(63) Perutz, M. F.; Johnson, T.; Suzuki, M.; Finch, J. T. *Proc. Natl. Acad. Sci. U.S.A.* **1994**, *91*, 5355–5358.
(64) DePace, A. H.; Santoso, A.; Hillner, P.; Weissman, J. S. *Cell* **1998**, *93*, 1241–1252.